



UNIVERSITY OF TWENTE.

Faculty of Engineering Technology

Design of a Sit-To-Stand Controller for a Lower Limb Exoskeleton and Validation by Feasible Crutch Usage Identification

E.V. Velu, BSc.

Master thesis Biomedical Engineering

12-12-2018

BW-640

Examination Committee:

dr.ir. A.Q.L. Keemink

dr. E.H.F. van Asseldonk

dr.ir. G.A. Folkertsma

Department of Biomechanical Engineering
University of Twente
P.O. Box 217
7500 AE Enschede
The Netherlands



Contents

	Page
1 Introduction	3
1.1 Background	3
1.2 Motion Analysis	4
1.3 Control Strategies	5
1.3.1 High-Level Controllers	5
1.3.2 Mid-Level Controllers	5
1.3.3 Low-Level Controllers	7
1.3.4 Conclusion	7
2 Paper	9
I Introduction	9
II Method	10
III Simulation Method	14
IV Results	15
V Discussion	18
References	19
3 Discussion	20
References	21

List of Abbreviations

ADL Activities of Daily Living

AIS ASIA Impairment Scale

ASIA American Spinal Injury Association

BoS Base of Support

CoF Coefficient of Friction

CoM Center of Mass

CoP Center of Pressure

DOBC Disturbance Observer-Based Control

HES Human Exoskeleton System

HKAE Hip-Knee-Ankle Exoskeleton

ILQR Iterative Linear Quadratic Regulator

MPC Model Predictive Control

NMC NeuroMuscular Controller

NMM NeuroMuscular Model

PID Proportional-Integral-Derivative

RoM Range of Motion

SCI Spinal Cord Injury

STS Sit-To-Stand

XCoM Extrapolated Center of Mass

1 Introduction

Exoskeletons can be promising to help Spinal Cord Injury (SCI) patients regain their mobility. To successfully develop an exoskeleton which can reduce the lifetime costs and improve life quality of the patient by improving the mobility, the exoskeleton has to be versatile. Because the Sit-To-Stand(STS) motion is used to initiate the use of an exoskeleton, it may be one of the most important tasks to make an exoskeleton successful. Moreover, the STS is one of the most challenging Activities of Daily Living (ADL), because it requires high joint torques and Range of Motion (RoM)[1]. Therefore, crutch usage is important to achieve sufficient force for a successful STS motion. The goal of this study is to design a STS controller for a Hip-Knee-Ankle Exoskeleton (HKAE) for SCI patients of ASIA Impairment Scale (AIS) class A and validate it by categorizing proper crutch usage in the sagittal plane. This study assumes the STS motion is sagittally symmetric. Furthermore, it is assumed that the feet and crutches remains flat and fixed to the floor. In the model fixed partial Center of Mass's (CoM) are used, while especially the CoM of the torso can shift significantly. While commonly known principles like the PD controller are used, the designed controller and model coded in Matlab simulated using Simulink's ODE45 solver is fully original.

This thesis contains a supplementary introduction and background information preliminary to a paper and an elaborated discussion subsequently to a paper. The introduction shows the background and importance of this project followed by an analysis of the STS motion. Furthermore, different control strategies are analyzed to make a substantiated control design choice. In the paper the method and results are presented and discussed.

1.1 Background

Exoskeletons can be divided into three categories based on their intended use and functions[2]. The first category focuses on performance augmentation of the healthy user. The other two categories focus on physically impaired users and can be divided in task performance assistance and therapeutic purposes. Task performance assistance focuses on reducing overall metabolic costs or time to increase task performance and therapeutic exoskeletons focuses on (non-) adaptive support, resist or perturbations in order to stimulate and train the user's input[2].

The American Spinal Injury Association (ASIA) published the AIS to categorize SCI patients. The most severe paraplegic class, patients without sensory or motor functions preserved in the sacral segments, is rated as AIS class A[3]. SCI can be subdivided in traumatic and non-traumatic SCI. Traumatic SCI is commonly caused by falls (53.0%), traffic (21.6%) or sports (14.1%) accidents[4]. Main causes for non-traumatic SCI are vascular diseases (27.9%), spinal degeneration (26.1%), inflammation (17.2%), malignant tumor (16.8%) and benign tumors- (11.2%)[5]. While traumatic lesions (54.7%) are almost as common as non-traumatic lesions in the Dutch and Flemish rehabilitation centers, most of the AIS class A cases are the result of a traumatic lesion (67.1%)[5].

The estimated incidence of traumatic SCI was 11.7 per million per year in the Netherlands in 2010[4], which would result in an AIS class A incidence of 6.5 per million per year with the ratio data given by Osterthun et al.[5]. AIS class A patients can have estimated lifetime costs up to \$2,391,872[6]. By multiplying the estimated lifetime costs with the annual incidence and the dutch population of roughly 17.2 million, the yearly costs of AIS class A patients can be estimated at \$267,411,290 (€229,973,709). By improving the mobility of AIS class A patients using a HKAE, the 1 year post-injury employment of 12%[6] and re-hospitalization of 30% may be improved, decreasing the average lifetime costs.

The Wearable Exoskeleton 2[7], one of the most powerful exoskeletons, developed as part of the Symbitron project is used in this study and will be referred to as the HKAE. While the used HKAE may be used for all three exoskeleton categories depending on the used controller, the HKAE with the controller presented is intended for task performance assistance for SCI patients of AIS class A. The ReWalk[8], Ekso[9] and Indego[10] are exoskeletons approved by U.S. Food and Drug Administration for use as rehabilitation devices, which all demonstrated successful STS capabilities[11]. The Rewalk uses a user-operated wrist pad to command sit to stand, stand to sit and walk activation[8].

1.2 Motion Analysis

To be able to correctly support the STS motion, the biomechanics of the STS motion is studied to fully understand the motion. In this section, besides the biomechanics of various subjects, computerized optimizations are discussed. STS performance can be more demanding than other ADL[1] requiring higher joint torques and RoM[13, 14, 15]. Because the STS motion requires these high performance characteristics, the exoskeleton can not totally support the STS and stability might become the main concern to successfully support STS.

Based on the horizontal and vertical velocities of the Center of Mass (CoM), the STS motion can be divided into three phases as can be seen in figure 1[12]. During the acceleration phase, the CoM accelerates in the horizontal plane. After acceleration, the velocity is redirected into a vertical velocity during the transition phase. In the final deceleration phase, the CoM moves vertically and decelerates till the stable standing position is reached. Although literature accurately describes the STS motion[12] and joint torques[14, 13], the stand-to-sit motion is not well studied.

Besides analyzing STS motions of varies subjects, STS can also be analyzed using STS computations. Using kinematic data, STS motions can be computed and analyzed using inverse dynamics[15]. While the computational analysis showed that the STS movement can be optimized to minimize either the maximum hip or knee torque to either 0.24 or 0.51 Nm kg^{-1} [15], subject studies show maximum hip torques of 0.914[13] $\text{Nm kg}^{-1} \text{ m}^{-1}$ to 0.98 Nm kg^{-1} [14] and maximum knee torques of 0.45 Nm kg^{-1} [14] to 1.170[13] $\text{Nm kg}^{-1} \text{ m}^{-1}$ respectively using inverse kinematics. Given a subject of 1.80m and the maximum allowable mass of 85kg, these relative torques can be converted into absolute maximum torques seen in table 1. Considering the HKAE of roughly 40 kg will increase these needed maximum torques by roughly 1.5, it can be stated that the technical specifications of the HKAE likely fall short in providing sufficient torque for a robust STS motion. However, crutches are used by the subject and the HKAE can be used to properly assist during the STS motion, minimizing the subject's effort or time. Hence the importance of the crutches to successfully complete the STS motion.

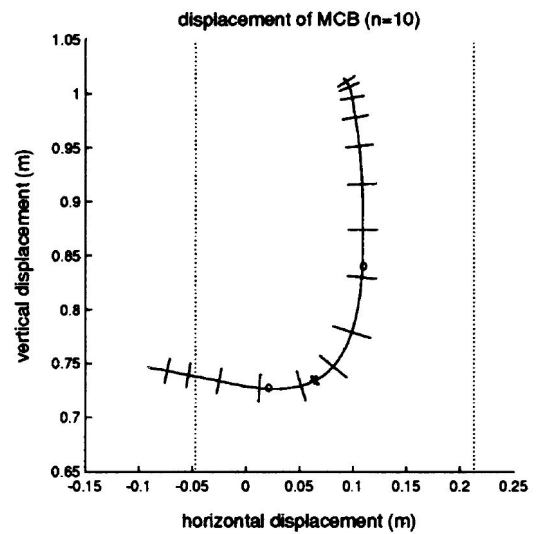


Figure 1: Mean of the CoM displacement from left to right during STS with standard error (n=10). Vertical dotted lines indicating the foot support base with the ankle joint in the coordinate system origin. The open dots divide the different phases with the asterisk indicating seat-off[12].

Table 1: Maximum total absolute joint torques needed for STS with a 1.80m and 85kg subject

	Knee Torque (Nm)	Hip Torque (Nm)
Subject studies[14, 13]	76.5 - 179	140 - 166.6
Optimization knee[15]	86.8	166.6
Optimization hip[15]	218	40.8
Technical specifications HKAE	140	200

1.3 Control Strategies

Because the usable in- and outputs are dependent on the used exoskeleton, possible control strategies highly depend on the exoskeleton used. The **HKAE** used in this project can measure the joint positions and torques, the joint velocities and accelerations can be estimated using the joint positions. The **HKAE** can be controlled using either joint positions or torques as control input.

Exoskeleton control strategies and evaluations vary widely and comparative studies of controllers are limited[2, 16]. Because different control strategy approaches may be useful for this goal, controllers intended for both **STS** or different **ADL** are studied. Although qualitative evaluations of control strategies are limited, controllers can be compared by estimating the robustness, predictability and computational intensity.

Hierarchical controllers can be subdivided into a high-, mid- and low-level controller[17]. The function of the high-level controller, also known as the perception layer, is to perceive the user's intention, in other words, activity recognition and human intent identification. Mid-level controllers can be subdivided in the trajectory and translation layer. The trajectory layer generates the trajectory according to the high-level controller output. Once the desired trajectory is obtained, the trajectory can be modified into motor input commands by the translation layer. Although the trajectory layer commonly describes the **CoM** trajectory, some describe the joint angle trajectories, force trajectory or position set-points which may not require the additional translation layer. Finally the low-level controller, also known as the execution layer, is responsible for correctly following the desired trajectory. This is generally done by minimizing the error of the desired and true trajectory by altering the motor input signals. While many different controllers are available, some controllers can only be used in combination with certain control strategies. The **HKAE** used in this study has an integrated disturbance observer-based low-level torque controller to minimize the effect of perturbations.

1.3.1 High-Level Controllers

The high-level controller detects the human intention by using the user's state and/or intent. Once the intention is determined, the high-level controller can regulate the use of the mid-level controllers. Because the high-level controller is considered to have the least effect on the motion performance, the literature focuses on the mid-level controller performance. Commonly the human intention is given via an user-operated control panel[8]. However, the sagittal rotation of the spine can also be used to detect **STS** intention. Moreover, force sensors in the crutches may be used in combination with angular data to activate the **STS**.

1.3.2 Mid-Level Controllers

Once the human intention is determined, the mid-level controller is activated according to the user's state and/or intent. Mid-level controllers can be divided in the trajectory and translation layer. The trajectory layer generates the trajectory according to the high-level controller output. Once the desired trajectory is obtained, the trajectory has to be modified into motor input commands by the translation layer. Although the trajectory layer commonly describes the **CoM** trajectory, some describe the joint angle trajectories, force trajectory or position set-points. Due to the different high-level outputs, some high-level mid-level combinations are not possible.

Trajectory Layer

Minimum Jerk Jerk is expressed as the time-derivative of the acceleration and is a good way to express the smoothness of a motion. Minimizing the jerk in a trajectory is an effective way to generate comfortable trajectories for human locomotion[18]. Using a fifth order polynomial with position, velocity and acceleration boundary conditions, a minimum jerk trajectory can be generated.

Model Predictive **Model Predictive Control (MPC)** uses basic descriptors to predict the outputs and future errors[19]. Using these predictions the **MPC** can generate online gait trajectories in real time, while taking predicted errors into account. Although this is successfully used for gait trajectory generation[19], the **MPC** is highly dependent on the model or model descriptors. While the **MPC** has been used for cyclic movements using model descriptors[19], it can also be used for a noncyclic **STS** motion using an accurate model. However, the **MPC** is highly dependent on the accuracy of the model. The **MPC** can generate the highest possible robustness, but is consequently limited by the high demand for computational power. Therefore, it is unlikely that **MPC** can be successfully used for the **STS** motion.

Motion Capture Data By analyzing the movements of a **STS** performance on healthy subjects using a motion capture system, reference trajectories can be generated[20]. Although the reference trajectories can be useful for the specific case it captured, it is case specific and depends on properties of subject, chair and environment. It can be stated that trajectories based on motion captured data are not adaptive to the situation and therefore not robust.

NeuroMuscular Model The **NeuroMuscular Controller (NMC)** uses the bio-inspired **NeuroMuscular Model (NMM)** proposed by Geyer and Herr [21] to derive the reference exoskeleton torque pattern[22]. It is shown that an adaptive **NMC** for a lower-limb exoskeleton can generate walking at different speeds with reasonably similar joint torques compared to healthy subjects[22]. The **NMC** requires only very few inputs and although only used for walking it demonstrated remarkable versatility[22] and may be used for **STS** control strategies. The advantages of the **NMC** include robustness, modularity and adaptability[22].

Stage Recognition Although a trajectory generating trajectory layer may be desired, set-points can be used to define the desired movement. Here the **STS** movement is divided in multiple stages, where each stage can have different mid- and low-level control strategies. While the set-points can already be used to move, a polynomial fit of the trajectory can smoothen the **STS** movement[23]. The stage recognition strategy is successfully used for a single-joint exoskeleton[24], but can induce adverse effects on stability and robustness when used for a multi-joint exoskeleton.

Stable Space A stable space controller focuses on a quasi-static stable trajectory. Although most controllers have a quasi-static stable trajectory, the stable space controller maximizes the margin for error by centering the **Center of Pressure** in the **Base of Support**. Since the **STS** has double support, the user's upper limb effort has to be taken into account to ensure stability.[25, 26] This method can adapt to the user's input, minimizing danger from improper crutch usage and stimulating proper crutch usage.[25] While stable space trajectories are similar to natural human motion, comparison shows more oscillatory and less conservative behaviour at natural human motion[26]. Stable space trajectory generation is a self-adaptive control method with a higher stability and reliability compared to traditional trajectory control methods[25].

Translation Layer

Impedance Commonly trajectories are expressed in the position domain. The mid-level controllers mentioned above are position controllers. Instead of controlling the positions of the **Human Exoskeleton System (HES)**, it is also possible to control the force interaction between the user and the exoskeleton. The forces are based on pre-specified values depending on the movement stage[2]. This strategy may take performance speed or initial conditions into account, but is difficult to optimize across multiple conditions[2].

Inverse Kinematics Using a simplified model of the **HES**, inverse kinematics can be used to find values of generalized coordinates given a desired **CoM**. Although simplified models are used, inverse kinematics can accurately generalize the angles using a given **CoM** trajectory[26, 27, 28]. Since the controller has to continuously calculate the angles using inverse kinematics, it may be computationally intensive. Inverse kinematics have been successfully used in combination with adaptive **Proportional-Integral-Derivative (PID)** controllers[20, 28] or an **Iterative Linear Quadratic Regulator (ILQR)** model[26, 27].

Trajectory Modification If joint trajectories are given by the trajectory layer e.g. motion capture data, effective joint trajectories can be made using simple modifications[20]. Here it is essential that the motion capture data is normalized to the measured subject's dimensions. Using the user's dimensions the motion capture data can be modified into effective joint trajectories[20].

Machine learning Machine learning is a novel technology which is increasingly used to control robotics. Machine learning requires a period of motion learning, where data of the current unassisted **STS** motion is captured e.g. wearing the exoskeleton in zero-impedance mode. Although in this stage the user is not yet able to perform the desired **STS** motion, the user is able to perform **STS** using solely crutches. Because the system will learn the performed motion, it learns an user-specific trajectory. Nevertheless, the **STS** motion learned may not be the desired trajectory to perform **STS** with exoskeleton assistance.

Momentum-Based Balance Momentum-based balance control regulates joint torques in order to follow the desired linear and angular momentum trajectories[29, 30]. Torque feedback of each actuator ensures the desired force generated by the balance controller[29]. This feedback is regulated by a **PID** controller according to the desired and measured force, but is also regulated by the joint velocity and a constant bias[29]. The momentum-based balance control is successfully used to balance perturbed humanoids[29]. Although momentum-based balance control is used to remain balanced at a fixed position, it may also be used to follow certain trajectories.

1.3.3 Low-Level Controllers

The low-level controller minimizes the error between the true and desired trajectories. Therefore the low-level controller can be seen as the feedback module of the controller. Although a [Disturbance Observer-Based Control \(DOBC\)](#) is already integrated in the [HKAE](#), an additional low-level controller may be necessary or desired.

Proportional-Integral-Derivative Traditionally [PID](#) controllers are used to minimize the error between the desired and generalized trajectories[20, 23, 24, 27]. Depending on the on the high-level controller, the [PID](#) controller can be either torque or angle oriented. An adaptive [PID](#) controller is similar to a [PID](#) controller, but contains location depending gain matrices with K_p , K_i and K_d values. Although the adaptive [PID](#) controller requires intensive tuning of the gain matrices, effective methods for tuning are available[23, 31].

Iterative Linear Quadratic Regulator The [ILQR](#) algorithm can be used for locally-optimal feedback control[32]. The [ILQR](#) requires to determine a [HES](#) specific cost-function[26, 27, 32]. Compared to other nonlinear optimal control algorithms, [ILQR](#) requires less computational time and fewer iterations[32]. However, compared to the adaptive [PID](#) controller the [ILQR](#) is computationally more intensive which can be problematic for embedded systems[27].

Disturbance Observer-Based Using the [DOBC](#) technique, external disturbances, unmodeled dynamics and system parameter perturbations can be take into account[33, 34]. These different types of disturbances are used as input to guarantee the desired dynamic performances of the nonlinear system[34]. [DOBC](#) can attenuate disturbances and improve system's robustness[33, 34]. [DOBC](#) is widely used for nonlinear systems requiring high-precision and anti-disturbance control.

1.3.4 Conclusion

The mid-level control strategies discussed are evaluated on robustness, predictability, computational intensity and proven results in literature. Furthermore, the controller's demands on the controlled device are argued in terms of actuation and sensory information. A summary of these results can be seen in table 2.

Because the torques seen in table 1 exceed the maximum actuation torque of the exoskeleton if its mass is included, it is known that the exoskeleton is not able to fully support the [STS](#) motion. In other words, the actuation (seen in table 2) is limited. However, the exoskeleton can deliver full sensory information.

When looked at possible trajectory-layer controllers in table 2, the [NeuroMuscular Model](#) and [Stable Space](#) controller have a high rated robustness. Although the [NMC](#) may stimulate a more natural movement[22], the high stability and predictability from the [Stable Space](#) controller is preferable[25]. The controller used in this study is inspired on the [Stable Space](#) principle, but also uses the concept of [Stage Recognition](#) to separate the horizontal and vertical phase.

The translation-layer controller has to be a controller with limited actuation needed. Position control translation-layers cannot guarantee the output position using a limited actuation device. However, force control translation-layers can still deliver a desired scaled force vector when boundary conditions are used. To have a more predictable output, a force control output is used in the controller presented in this study.

Table 2: Comparison of control strategies found in literature. Trajectory layer controllers are controllers generating or selecting trajectories. Translation layer controllers can be used to execute the trajectory layer differently.

Trajectory Layer		Robustness	Predictability	Computational Intensity	Information Needed	Literature
	Minimum Jerk	Low	High Trajectory generated using polynomial.	Low	Full	Successfully used for smooth turning manoeuvres[18]
	Model Prediction	High	Low Trajectory generated using basic descriptors.	Very High Large computation time[19]	Full	Successfully used for gait trajectory generation[19], noncyclic movements (STS) may be difficult.
	Motion Capture Data	Low Case specific and unadaptable[20]	High Predefined trajectory normalized by initial conditions	Low Minimal real time computation	Full	Successfully tested on healthy subjects with case specific STS data[20]
	NeuroMuscular Model	High Simplified reflex model for adaptability[22]	Low Simplified bio-inspired model to generate CoM trajectory	High Extensive NMM resulting in high computational intensity	Full	Successfully tested on SCI subjects for walking with body weight support[22]
	Stage Recognition	Low Can have adverse robustness effects when used on multi-joint exoskeleton	High Predefined set points normalized by initial conditions	Low Minimal real time computation	Limited	Successfully tested with single-joint exoskeleton [24]
	Stable Space	High Maximized margin of CoM error Self-adaptive[26, 25]	High Simplified HES model to generate quasi-static stable CoM trajectory	High Computationally intensive for on-board systems[26]	Full	Successful STS of paraplegic patients when used on exoskeleton[25]
Translation Layer		Robustness	Predictability	Computational Intensity	Actuation Needed	Literature
	Momentum-Based Balance	High Linear and angular regulated momentum	High	Low Computational efficient[30]	Limited	Successfully used to balance humanoid robots[29, 30]
	Trajectory Modification	Low	High	Low	Full	
	Force-based Open-loop	Low	High	Low	Limited	Difficult to optimize across multiple conditions[2]
	Machine Learning	Low	Low	High	Full	

Design of a Sit-To-Stand Controller for a Lower Limb Exoskeleton and Validation by Feasible Crutch Usage Identification

Ewoud Velu, BSc.*; dr.ir. A.Q.L. Keemink*, dr. E.H.F. van Asseldonk*, dr.ir. G.A. Folkertsma†

December 12, 2018

Abstract

Lower limb exoskeletons can help to reduce the long term impact of spinal cord injury towards lifetime costs and life quality of the patient by improving the mobility. The versatility of exoskeletons is crucial to successfully achieve these goals. The sit-to-stand (STS) motion is essential for the use and versatility of exoskeletons. However, exoskeletons are not yet strong enough to fully execute the STS motion and therefore proper crutch usage is necessary. The goal of this study is to design a STS controller and to identify proper crutch usage according to crutch placement and angle orientation. We designed a controller which focuses on balancing the center of mass of the human exoskeleton system's (HES), while relying on the crutch forces to achieve sufficient upward force for successful STS motion. In this study the technical specifications of the Wearable Exoskeleton 2, one of the strongest exoskeletons, are used to simulate the effects of different crutch scenarios. The used HES model is a sagittal symmetric model with fixed ground contact points. This study presents the design of a STS controller for a lower limb exoskeleton and validates the feasibility of the designed STS controller, while identifying the contribution of the crutches.

I Introduction

Class A[1] of *ASIA Impairment Scale (AIS)* is the most severe paraplegic class and indicates the patients without any sensory or motor functions preserved in the sacral segments. These patients have a reduced mobility, which bothers them during *Activities of Daily Living (ADL)*. Exoskeletons can help these patients to increase their mobility and life comfort and to reduce their lifetime costs. By multiplying the estimated lifetime costs[2] with the annual incidence[3, 4] and the dutch population of roughly 17.2 million, the annual costs of AIS class A patients in the Netherlands can be estimated at \$267 million (€229 million). The goal of task performance assistance exoskeletons is to improve the mobility of *Spinal Cord Injury (SCI)* patients. By improving the mobility of AIS class A patients using an exoskeleton, the 1 year post-injury employment of 12%[2] and re-hospitalization of 30% may be improved, decreasing the average lifetime costs. The exoskeleton used in this study is designed for task performance assistance for SCI patients of AIS class A[1].

The *Sit-To-Stand (STS)* motion is essential to be able to use exoskeletons and is an important motion during *ADL*. Therefore, it is one of the most important tasks for the exoskeleton. The *Wearable Exoskeleton 2*[5] developed as part of the *Symbitron* project is used in this study and will be referred to as the *Hip-Knee-Ankle Exoskeleton (HKAE)*. The *ReWalk*[6], *Ekso*[7] and *Indego*[8] are exoskeletons approved by U.S. Foods and Drug Ad-

ministration for use as rehabilitation devices. These exoskeletons demonstrated successful *STS* capabilities while using crutches[9]. The *Rewalk* uses an user-operated wrist pad to command sit to stand, stand to sit and walk activation[6]. Although these exoskeletons prove the feasibility of a *STS* motion with an exoskeleton, it is unknown how the crutches are used. All successful *STS* motions executed by exoskeletons are supported by crutches, because proper crutch usage is critical for a successfully *STS* motion. However, only little is known about proper crutch usage.

The *STS* motion is one of the most demanding *ADL*[10] requiring high joint torques and *Range of Motion (RoM)*[11, 14, 15]. To be able to correctly support the *STS* motion, the biomechanics of the motion is studied extensively. Based on the horizontal and vertical velocities of the *Center of Mass (CoM)*, the *STS* motion can be divided into three phases. During the acceleration phase, the *CoM* accelerates forwards in the horizontal plane. After acceleration, the velocity is redirected into a vertical velocity during the transition phase. In the final deceleration phase, the *CoM* moves vertically and decelerates till the stable standing position is reached.

Besides analyzing *STS* motions of varies subjects, *STS* can also be analyzed using *STS* simulations. *STS* motions can be computed and analyzed using inverse dynamics, which uses kinematic data to calculate joint torques. Studies from Mak et al.[11] and Sibella et al.[12] calculated the maximum relative knee and hip torques using subject data. Yoshioka et al.[13] optimized the *STS* motion using computational analysis to minimize the maximum relative hip or knee torque (Nm/kg). Given a sub-

*Department of Biomechanical Engineering, University of Twente

†Department of Robotics and Mechatronics, University of Twente

Table I: Maximum total absolute joint torques (Nm) needed for STS with a 1.80m and 85kg subject with a 40kg exoskeleton

	Knee Torque	Hip Torque
Subject studies[11, 12]	113 - 263	206 - 245
Optimization knee[13]	127.5	245
Optimization hip[13]	320	60
Technical specifications HKAE[5]	140	200

ject of 1.80m and the maximum allowable mass of 85kg with an exoskeleton mass of 40kg, these relative torques can be converted into absolute maximum torques seen in table I. The technical specifications of the HKAE fall short in providing sufficient torque for a robust STS motion. However, the HKAE can be used to properly assist the STS motion, minimizing the subject's effort or STS time.

The HKAE used in this project can measure the joint angles and joint torques, which can be used as input for the controller. These measured joint angles can be derived into joint angle velocities over time. A stage recognition controller divides the operational space in stages using predefined set-points. The controller switches in chosen characteristics depending on the current stage. This is desired to be able to split the control method in a horizontal and vertical phase as mentioned above. The Center of Pressure (CoP) should remain within the Base of Support (BoS) to ensure stability. A stable space controller focuses on maintaining margin for CoP change within the BoS and thereby maintaining stability. This desired margin functions as a buffer for perturbations, incorrect assumptions and changes in crutch forces. In addition, the margin is desired because the crutch forces, which are essential for the STS motion, also have a horizontal component which may move the CoP towards the BoS limits. An impedance translation layer, similar to a Proportional-Derivative low-level controller, generates a desired end-effector force based on predefined values and desired trajectory points. The controller presented in this study uses the mentioned principles, stage recognition, stable space and impedance translation, to design a STS controller.

This study focuses on the design of a simple controller to overcome the limited force actuated situation, while using the technical specifications of one of the strongest exoskeletons. Furthermore, this study shows the importance of proper crutch usage for STS performance and the user's safety during the STS motion. The goal of this study is to design and validate a STS controller for a HKAE for SCI patients of AIS class A. The controller is validated by determining a feasible region for crutch usage in terms of crutch placement and angle orientation in a simulation setting using computational analysis. The modeled crutches are simplified to a spring-damper model to be able to determine this feasible region. The model used for this study is a sagittal symmetric model, which does not take possible slip or roll-over of the feet and crutches into account. However, it is calculated which cases can be neglected due to the possible slip.

II Method

Control Design The controller will have to move the subject's CoM towards the feet until stability can be guaranteed for the vertical motion. Therefore, the controller is split into two stages which differ in control characteristics, similar to the first two phases of the human STS motion. The stage specific control characteristics are the BoS, controllable points and the desired reference positions of the controllable points. These control characteristics are further elaborated in the next paragraphs.

During the first control stage, the CoM moves towards the feet until the Extrapolated Center of Mass (XCoM elaborated in the third paragraph) is located in the BoS, resulting in the initiation of the second stage. During the second stage the exoskeleton will help the subject to rise as much as possible in the vertical stage while focusing on balancing the subject.

The controller can be separated into six blocks (figure I a-f) and is combined with a model of the Human Exoskeleton System (HES), crutches and sofa (figure I g-i). These six controller blocks combined, result in the desired joint torques, which are constrained by the software limitations in terms of RoM and maximum joint torque magnitude (block f). The hardware endstops are implemented in the HES (block g). The values of these soft- and hardware limits are presented in table II. All equations presented in this section refer to the reference positions and angles presented in figure II.

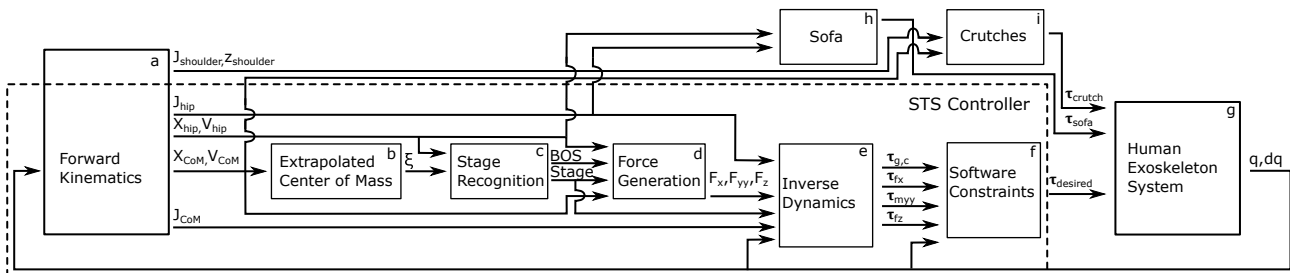


Figure I: Schematic representation of the used STS controller and HES model. The first block calculates the hip and CoM coordinates and Jacobians using forward kinematics. The XCoM is calculated using the CoM position and velocity. From the XCoM and hip coordinates, the stage and thus the BoS is determined. The reference points, depended on the stage, are used to calculate the forces using corresponding PD gain matrices. Inverse dynamics is used to counteract the dynamics of the exoskeleton and generate the desired resulting forces by prioritizing the torques.

Table II: Software and hardware angle limitations of the used HKAE in $^\circ$ with respect to figure II and the maximum total joint torque magnitudes in Nm

	Software Limitations		Hardware Endstops		Joint Torque Magnitude
	Min	Max	Min	Max	Max
Hip	-11	138	-14	140	200
Knee	-103	0	-105	3	140
Ankle	-30	32	-33	34	200

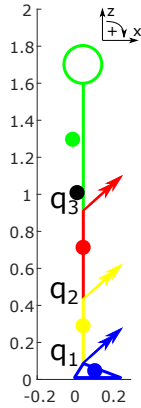


Figure II: Simplified kinematic diagram of the human exoskeleton system with the colored dots representing the respective partial CoM's and the total CoM in black, q_1 , q_2 and q_3 represent the actuated ankle, knee and hip joint at reference angle zero. The partial CoM of the torso is located behind the torso, due to the heavy exoskeleton's backpack estimated at 15kg and 0.2m behind the torso's CoM.

Forward Kinematics The controller starts with the forward kinematics (figure 1a), which calculates the hip and CoM coordinates and corresponding Jacobians. The hip and CoM coordinates are required as controllable points and are needed to determine the current stage. The Jacobians are needed to translate the end-effector forces into joint torques. The CoM is approximated using the model of the Caucasian male designed by Nikolova et al.[14]. This model is adjusted to the subject's mass and length chosen at 85kg and 1.80m, similar to the maximum specifications of the HKAE.

Equation I calculates the hip coordinates x and z , presented as the position of the hip (\mathbf{P}_{hip}). The ankle position with respect to the heel position can be expressed by x_{ankle} and z_{ankle} . The knee position with respect to the ankle position can be expressed by the reference position L_{shank} in combination with the rotation matrix of the shank with respect to the heel (dependent on the ankle angle, q_1). The hip position with respect to the knee position can be expressed by the reference position L_{thigh} in combination with the rotation matrix of the thigh with respect to the heel (dependent on q_1 and the knee angle, q_2). Therefore, \mathbf{P}_{hip} can be calculated using the current angles and the predefined reference positions.

The Jacobian (\mathbf{J} in equation II) can be derived using the corresponding position. \mathbf{J}_{hip} is calculated using \mathbf{P}_{hip} . The CoM position and its Jacobian are calculated in a similar manner, using the partial CoMs.

$$\mathbf{P}_{hip} = \begin{bmatrix} x_{ankle} \\ z_{ankle} \end{bmatrix} + \mathbf{R}_0^1(q_1) \begin{bmatrix} 0 \\ L_{shank} \end{bmatrix} + \mathbf{R}_0^2(q_1, q_2) \begin{bmatrix} 0 \\ L_{thigh} \end{bmatrix} \quad (I)$$

$$\mathbf{J} = \frac{\partial \mathbf{P}}{\partial \mathbf{q}_{1,2,3}} \quad (II)$$

Extrapolated Center of Mass The XCoM is defined as the point to which the horizontal position of the CoM converges, taking the CoM's angular velocity into account[15]. If the XCoM is behind or in front of the BoS the CoM will respectively fall back or fall in front of the BoS. The XCoM (ξ in equation III) can predict stability conditions using the eigenfrequency of the HES, while the CoM only describes stability for static balance[15]. The XCoM can guarantee stability if located within the BoS[15]. The XCoM (figure 1b) is calculated using the CoM's horizontal position (x_{CoM}), horizontal velocity (\dot{x}_{CoM}) and the eigenfrequency (ω_0) of the HES. The eigenfrequency of the HES (equation IV) is calculated using the gravitational acceleration (g) and the pendulum length ($l(q)$). $l(q)$ is the length of a simplified pendulum defined by the distance of the CoM with respect to the ankle joint, which is dependent on the joint angles (q). The XCoM can promote an earlier prediction of the stability. Therefore, it is used to initiate the second stage of the controller and results in an earlier and valid seat-off compared to the use of the CoM.

$$\xi(\mathbf{q}, \dot{\mathbf{q}}) = x_{CoM}(\mathbf{q}) + \frac{\dot{x}_{CoM}(\dot{\mathbf{q}})}{\omega_0(\mathbf{q})} \quad (III)$$

$$\omega_0(\mathbf{q}) = \sqrt{g/l(\mathbf{q})} \quad (IV)$$

Stage Recognition The stage recognition block (figure 1c) generates two outputs, the definition of the stage and the corresponding BoS. The BoS is dependent on the stage of the motion. In the first stage, the BoS includes both the sofa and feet. In the second stage, the BoS is only defined by the feet.

The stage recognition principle determines the stage using the XCoM and horizontal hip position. The second stage is initiated if the XCoM is within the second BoS, defined by the feet. However, the second stage is also initiated if the horizontal position of the hip (x_{hip}) passes a threshold of 10 cm behind the heel. This to ensure the subject does not fall of the chair without initiating the second stage.

Force Generation The force generation block (figure 1d) calculates the desired end-effector forces using the reference trajectories and a spring-damper concept. Commonly the CoM position (x_{CoM} and z_{CoM}) is used as controllable position. However, during the first stage the vertical position of the hip (z_{hip}) is controlled instead of vertical position of the CoM (z_{CoM}). Furthermore, the angle of the torso (q_{torso}) is used as controllable angle in both stages. The first stage controls the horizontal position of the CoM (x_{CoM}), z_{hip} and q_{torso} , the second stage

controls x_{CoM} , z_{CoM} and q_{torso} . Both stages use a spring-damper system (PD) to follow the desired trajectories or end-points, resulting in forces located on the CoM and/or hip and a moment on the torso.

The different, not commonly used, vertical controllable point (z_{hip}) in the first stage is chosen because this stage focuses on the horizontal movement while remaining seated. Therefore, the desired trajectory of z_{hip} during the first stage is known, while the trajectory of z_{CoM} is a result of the known desired z_{hip} and the global angle of the torso (q_{torso} expressed as $q_1 + q_2 + q_3$). However, during the second stage the control of z_{hip} does not suffice, because it is necessary to raise z_{CoM} towards the standing configuration.

The minimum jerk trajectory is calculated using the scenario-specific initial conditions and desired end values as boundary conditions. A fifth order polynomial is used to calculate this minimum jerk trajectory as expressed in equation V.

$$\mathbf{P}_{\text{ref}}(t) = \sum_{n=0}^5 a_n t^n \quad (\text{V})$$

In the first stage, the minimum jerk trajectory is generated using the case specific measured initial conditions, the respective desired end positions (x_{ankle} , z_{sofa} and 50°), end velocities ($\mathbf{V}_{\text{end}} = 0$) and end accelerations ($\mathbf{a}_{\text{end}} = 0$). x_{ankle} is chosen as the desired x_{CoM} position to be able to move the CoM forward and initiate the second stage. z_{sofa} (the height of the sofa) is chosen as the desired z_{hip} to push the subject slightly out of the sagged sofa to reduce the sofa friction. Considering a horizontal thigh while seating, the local hip angle equals 90° , in order to maintain a global angle of zero $^\circ$. It is desired to move the torso as much forward as possible. Therefore, the maximum hip flexion of the HKAE of 140° results in the maximum global torso angle of 50° and is chosen as the desired torso angle.

During the second stage, the minimum jerk trajectory is generated using the previous end conditions as start conditions and using the new desired end positions x_{ankle} , $z_{\text{com,reference}}$ and q_{zero} . However, for the z_{com} start condition the vertical position of the CoM at the sitting configuration is used. This is done because the controllable vertical point is changed and therefore the previous end-point of z_{hip} can not be used as start point for z_{com} . It is desired to maximize the error margin of the CoM within the BoS, therefore a vertical trajectory constrained above the ankle joint is generated to move the CoM reference position upward. Because the partial CoM of the torso is slightly behind the torso (figure II), the angle of the torso at which the partial CoM is above the hip joint is not equal to zero and defined as q_{zero} . This angle is used as desired angle end position. $z_{\text{com,reference}}$ is z_{com} at the reference position (figure II) with the hip angle (q_3) equal to q_{zero} .

The force is generated using the controllable positions (\mathbf{P}), controllable velocities ($\dot{\mathbf{P}}$), the desired previous mentioned trajectory points ($\mathbf{P}_{\text{spring}}$) in a stiffness-damper mechanism (equation VI). Using the boundary condition

(equation VII) derived from figure III, the stiffness gain (K_p in equation VIII) is calculated. Here, p_{spring} represents the desired trajectory position and p_{max} represents the position at which the maximum spring force (F_{max}) is generated. To generalize the behaviour of the exoskeleton towards different subjects, the force is derived into an acceleration (a_{max}) by element wise dividing the force with the HES's mass (m_{hes}). The damper gain is calculated using the definition of critical damping ($K_{d,\text{critical}}$ in equation IX). The used stiffness and damper gains are presented in table III. The end-effector force resulting from the stiffness component ($K_p(P_{\text{spring}} - P)$) is limited to the magnitude of F_{max} . Furthermore, the vertical force resulting from the stiffness component is limited to a positive force, because it is never desired to push the HES downward during the STS motion.

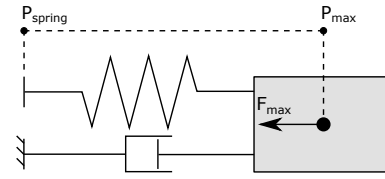


Figure III: Kinetic diagram of the spring-damper system used to calculate the stiffness gain K_p

$$\mathbf{F} = \mathbf{K}_p(\mathbf{P}_{\text{spring}} - \mathbf{P}) + \mathbf{K}_d(-\dot{\mathbf{P}}) \quad (\text{VI})$$

$$F_{\text{max}} = m_{\text{hes}} a_{\text{max}} = K_p(p_{\text{spring}} - p_{\text{max}}) \quad (\text{VII})$$

$$K_p = \frac{m_{\text{hes}} a_{\text{max}}}{p_{\text{spring}} - p_{\text{max}}} \quad (\text{VIII})$$

$$K_{d,\text{critical}} = 2\sqrt{K_p m_{\text{hes}}} = 2m_{\text{hes}} \sqrt{\frac{a_{\text{max}}}{p_{\text{spring}} - p_{\text{max}}}} \quad (\text{IX})$$

Table III: Resulting stiffness and damping coefficients for different accelerations (a_{max})

	$a_{\text{max}} = 2 \text{ m/s}^2$		$a_{\text{max}} = 4 \text{ m/s}^2$	
	K_p	K_d	K_p	K_d
Fx	4683 N/m	1432 Ns/m	9366 N/m	2025 Ns/m
Fz	1095 N/m	692 Ns/m	2189 N/m	979 Ns/m
My	300 N/rad	362 Ns/rad	599 N/rad	512 Ns/rad

Inverse Dynamics In the inverse dynamics block (figure Ie) the dynamics of the HES are counteracted and the desired-end effector forces are calculated into the desired torques using the corresponding Jacobians (\mathbf{J}). Commonly, the torques ($\boldsymbol{\tau}$) are calculated by counteracting the model dynamics (the inertia term $\mathbf{M}(\mathbf{q})\ddot{\mathbf{q}}$, gravity balance term $\tilde{\mathbf{g}}(\mathbf{q})$ and the Coriolis and centripetal term $\tilde{\mathbf{c}}(\mathbf{q}, \dot{\mathbf{q}})$ in equation X) and subsequently adding the torques corresponding to the desired end-effector forces ($\mathbf{J}_{\text{EE}}^T(\mathbf{q})F_{\text{EE}}$ in equation X). In this study the acceleration term of the dynamics is neglected due to the poor accuracy of the acceleration, which has to be derived real-time from the measured exoskeleton's angles.

The HES's dynamics are counteracted by the gravity balance, Coriolis and centripetal terms. By adding the end effector forces generated in the force generation block

and multiplying them with their corresponding Jacobian (\mathbf{J}), all these terms (resulting in partial torques) can be composed into the total desired torques. During the first stage the desired torques can be expressed as $\tau_{\text{des,stage1}}$ in equation XI. And during the second stage the desired torques can be expressed as $\tau_{\text{des,stage2}}$ in equation XII. These desired torques are vectors containing the ankle, knee and hip torques.

$$\tau = \tilde{\mathbf{M}}(\mathbf{q})\ddot{\mathbf{q}} + \tilde{\mathbf{g}}(\mathbf{q}) + \tilde{\mathbf{c}}(\mathbf{q}, \dot{\mathbf{q}}) + \mathbf{J}_{\text{EE}}^{\top}(\mathbf{q})\mathbf{F}_{\text{EE}} \quad (\text{X})$$

$$\tau_{\text{des,stage1}} = \tilde{\mathbf{g}}_{\text{hes}}(\mathbf{q}) + \tilde{\mathbf{c}}_{\text{hes}}(\mathbf{q}, \dot{\mathbf{q}}) + \mathbf{J}_{\text{CoM}}^{\top}(\mathbf{q})F_{x,\text{CoM}} + \mathbf{J}_{\text{hip}}^{\top}(\mathbf{q})F_{z,\text{hip}} + \mathbf{J}_{\text{torso}}^{\top}(\mathbf{q})M_{\text{torso}} \quad (\text{XI})$$

$$\tau_{\text{des,stage2}} = \tilde{\mathbf{g}}_{\text{hes}}(\mathbf{q}) + \tilde{\mathbf{c}}_{\text{hes}}(\mathbf{q}, \dot{\mathbf{q}}) + \mathbf{J}_{\text{CoM}}^{\top}(\mathbf{q})F_{x,\text{CoM}} + \mathbf{J}_{\text{CoM}}^{\top}(\mathbf{q})F_{z,\text{CoM}} + \mathbf{J}_{\text{torso}}^{\top}(\mathbf{q})M_{\text{torso}} \quad (\text{XII})$$

Software Constraints The software limitations and maximum joint torque magnitude of the exoskeleton have to be taken into account in the controller's software. This is realized in the software constraints block (figure 1f). The exoskeleton will be, at some point, likely to fall short to generate the required torques for the HES to perform the STS motion. Therefore, in the software the limitations are taken into account to use the joint actuators as desired as possible. The resulting ankle, knee and hip torques of the three end-effector forces, the horizontal force (τ_{F_x}), the vertical force (τ_{F_z}) and the sagittal moment (τ_{M_y}), are separate terms as seen in equation XIII.

$$\tau_{\text{desired}} = \begin{bmatrix} \tau_{\text{desired,ankle}} \\ \tau_{\text{desired,knee}} \\ \tau_{\text{desired,hip}} \end{bmatrix} = \tau_{\tilde{c}} + \tau_{F_x} + \tau_{M_y} + \tau_{F_z} + \tau_{\tilde{g}} \quad (\text{XIII})$$

If the total sum exceeds the maximum torque magnitude of one of the exoskeleton's joints, the desired torques are scaled down in a prioritized order as presented in equation XIV. The terms are separated to be able to prioritize the torques. The torques resulting from counteracting the Coriolis and centrifugal effects ($\tau_{\tilde{c}}$) are not scaled down, because these torques are considerably low and important to be able to negate Coriolis and centrifugal effects. The main goal of the exoskeleton is to balance the HES with the horizontal end-effector force (using τ_{F_x}). Therefore, τ_{F_x} is prioritized as an important torque vector and will be maintained as long as possible. The moment on the torso (τ_{M_y}) is used to realize the correct configuration of the HES and therefore also contributes to the balancing of the HES. Therefore, besides τ_{F_x} , τ_{M_y} is important to balance the HES. Lastly, the torques resulting from the vertical forces (vertical end-effector force τ_{F_z} and gravity balance force $\tau_{\tilde{g}}$) are scaled down first. This is chosen, because these torques are less important to maintain the balance of the HES and are the most demanding torques. In most scenarios, lowering the most demanding torques (τ_{F_z} and $\tau_{\tilde{g}}$) will be sufficient to ensure that the maximum joint torque magnitudes (τ_{max}) are not exceeded.

The gains (K_1 , K_2 and K_3) are calculated in order to scale down the partial joint torques to satisfy the maximum joint torque magnitudes. The gains (K_1 , K_2 and K_3) are the minimum values from the gain vectors (\mathbf{K}_1 , \mathbf{K}_2 and \mathbf{K}_3) to ensure all three joint torque magnitudes are satisfied (equation XVIII, XIX and XX). The gains are calculated for each joint, by dividing the remaining joint torque without the scalable term (till τ_{max}) by the corresponding scalable joint torque (equation XV, XVI and XVII). In this equations $A \oslash B$ is used, where \oslash denotes the Hadamard (element-wise) division. The gains are used in the mentioned prioritizing method, where the terms are scaled down until the maximum joint torque magnitudes are satisfied. If the first gain (K_1) is lower than 1, it scales the last term ($\tau_{F_z} + \tau_{\tilde{g}}$) down until this gain reaches zero. If this gain goes below zero, the next gain (K_2) is used to scale τ_{M_y} down. If this gain also reaches zero the last gain (K_3) scales τ_{F_x} down until the maximum joint torque magnitudes are satisfied (equation XIV).

$$\tau_{\text{desired}} = \tau_{\tilde{c}} + K_3\tau_{F_x} + K_2\tau_{M_y} + K_1(\tau_{F_z} + \tau_{\tilde{g}}) \quad (\text{XIV})$$

$$\mathbf{K}_1 = (\tau_{\text{max}} - (\tau_{\tilde{c}} + \tau_{F_x} + \tau_{M_y})) \oslash (\tau_{F_z} + \tau_{\tilde{g}}) \quad (\text{XV})$$

$$\mathbf{K}_2 = (\tau_{\text{max}} - (\tau_{\tilde{c}} + \tau_{F_x})) \oslash \tau_{M_y} \quad (\text{XVI})$$

$$\mathbf{K}_3 = (\tau_{\text{max}} - \tau_{\tilde{c}}) \oslash \tau_{F_x} \quad (\text{XVII})$$

$$K_1 = \begin{cases} 1 & \text{if } 1 < \min(\mathbf{K}_1) \\ \min(\mathbf{K}_1) & \text{if } 0 \leq \min(\mathbf{K}_1) \leq 1 \\ 0 & \text{if } \min(\mathbf{K}_1) < 0 \end{cases} \quad (\text{XVIII})$$

$$K_2 = \begin{cases} 1 & \text{if } 1 < \min(\mathbf{K}_2) \quad \text{OR } 0 < K_1 \\ \min(\mathbf{K}_2) & \text{if } 0 \leq \min(\mathbf{K}_2) \leq 1 \quad \text{AND } 0 = K_1 \\ 0 & \text{if } \min(\mathbf{K}_2) < 0 \quad \text{AND } 0 = K_1 \end{cases} \quad (\text{XIX})$$

$$K_3 = \begin{cases} 1 & \text{if } 1 < \min(\mathbf{K}_3) \quad \text{OR } 0 < K_2 \\ \min(\mathbf{K}_3) & \text{if } 0 \leq \min(\mathbf{K}_3) \leq 1 \quad \text{AND } 0 = K_2 \\ 0 & \text{if } \min(\mathbf{K}_3) < 0 \quad \text{AND } 0 = K_2 \end{cases} \quad (\text{XX})$$

Human Exoskeleton System The HES is simulated using the Euler-Lagrange equations and applying external torques (figure 1g). From these equations the joint accelerations can be calculated using the external joint torques as input. The used external joint torques are the summation of the desired joint actuation torques (τ_{desired}), the joint torques resulting from the modeled sofa (τ_{sofa}), the joint torques resulting from the modeled crutch forces (τ_{crutch}) and the torques resulting from the passive human damping of the joints. All three joints are damped with a damping coefficient similar to the human joints, which is 0.1 Nms/rad[16].

Sofa The sofa is modeled using a vertical spring-damper model and a horizontal stick-slip model (figure

lh). The vertical spring-damper model uses the stroke of the sofa (estimated at 0.2m) where the gravitational force of the HES is in equilibrium ($a_{\max} = 9.81 \text{ m/s}^2$). This length ($p_{\text{spring}} - p_{\max}$) and acceleration are used to calculate the stiffness and damping gains (K_p and K_d in equations VIII and IX). The contact point of the HES is defined by the position of the hip (z_{hip}) with radius (r_{hip}) of 0.1m. The vertical sofa force (F_z) is calculated using the hip contact point's position ($z_{\text{hip}} - r_{\text{hip}}$), vertical velocity (\dot{z}_{hip}) and the mentioned gains (K_p and K_d) in equation XXI.

The horizontal stick-slip model is split into a static (stick) and kinetic (slip) friction force calculation. The static force calculation is used until the hip velocity exceeds the arbitrary threshold (V_{slip}) of 0.01 m/s. Thereafter, the kinetic force calculation is used to define the horizontal friction force. For the stick-slip model the static and kinetic friction values of fabric to fabric ($\mu_{\text{stat}} = 1.152$ and $\mu_{\text{kin}} = 0.823$ [17]) and an arbitrary viscous component ($\eta_{\text{vis}} = 0.5 \text{ Ns/m}$) are used. The static horizontal friction force ($F_{x,\text{stat}}$) is calculated using the normal force (F_z), the static friction coefficient (μ_{stat}) and the relative vertical hip velocity ($\dot{z}_{\text{hip}}/\dot{z}_{\text{hip,slip}}$) in equation XXII. The kinetic friction is calculated using the kinetic friction term ($-\text{sgn}(\dot{x}_{\text{hip}})\mu_{\text{kin}}F_z$) and the viscous friction term ($-\eta_{\text{vis}}\dot{x}_{\text{hip}}$) in equation XXIII.

The sofa forces are only present if the circle around the hip, defined by r_{hip} of 0.1m, makes contact with the sofa. Therefore, the vertical spring component is limited to a positive force. Using the Jacobian transpose of the hip, the joint torques (τ_{sofa}) corresponding with the sofa forces can be calculated.

$$F_z = K_p (P_{\text{spring},z} - (z_{\text{hip}} - r_{\text{hip}})) - K_d \dot{z}_{\text{hip}} \quad (\text{XXI})$$

$$F_{x,\text{stat}} = -\mu_{\text{stat}} F_z \frac{\dot{z}_{\text{hip}}}{\dot{z}_{\text{hip,slip}}} \quad (\text{XXII})$$

$$F_{x,\text{kin}} = -\text{sgn}(\dot{x}_{\text{hip}})\mu_{\text{kin}}F_z - \eta_{\text{vis}}\dot{x}_{\text{hip}} \quad (\text{XXIII})$$

Crutches The crutches have to be implemented in the simulations to be able to simulate successful STS motions (figure li). Using a constant force to model the crutches, the different crutch scenarios can be well compared. However, analysis of subjects show that the crutch force is not a constant force and varies from subject to subject[18]. Therefore it is chosen to design a simple model of the crutches, which is dependent on the pace (defined by the CoM's velocity) and progress (defined by the shoulder's height) of the STS motion.

To make a model of the crutches where different scenarios can still be compared, the crutch force is modeled using a constant force which linearly scales down after a certain CoM velocity and/or shoulder height threshold is reached (using K_{damping} and $K_{\text{completion}}$ equation XXIV). The crutch force is linearly damped after exceeding the common maximum STS velocity of 0.35 m/s[19] until the double velocity of 0.7 m/s is reached (equation XXV). Furthermore, the force is linearly scaled down when the shoulder height reaches 90% of the reference shoulder height until the fully stretched reference position

($z_{\text{shoulder,ref}}$ in equation XXVI). By choosing these factors to scale down the crutch force, the resulting crutch force reduces when the velocity is sufficient and when the standing position is approached. Using the Jacobian transpose of the shoulder, the joint torques (τ_{crutch}) corresponding with the crutch forces can be calculated and added to the HES.

$$F_{\text{crutch}} = F_{\text{crutch,max}} K_{\text{damping}} K_{\text{completion}} \quad (\text{XXIV})$$

$$K_{\text{damping}} = \begin{cases} 1 & \text{if } V_{\text{CoM}} < 0.35 \text{ m/s} \\ \frac{0.7 - V_{\text{CoM}}}{0.35} & \text{if } 0.35 \leq V_{\text{CoM}} \leq 0.7 \text{ m/s} \\ 0 & \text{if } 0.7 \text{ m/s} < V_{\text{CoM}} \end{cases} \quad (\text{XXV})$$

$$V_{\text{com}} = \begin{cases} \sqrt{\dot{x}_{\text{CoM}}^2 + \dot{z}_{\text{CoM}}^2} & \text{if } 0 \leq \dot{z}_{\text{CoM}} \\ \dot{x}_{\text{CoM}} & \text{if } \dot{z}_{\text{CoM}} < 0 \end{cases} \quad (\text{XXVI})$$

$$K_{\text{completion}} = \begin{cases} 1 & \text{if } z_{\text{sh}} < 0.9z_{\text{sh,ref}} \\ \frac{z_{\text{sh,ref}} - z_{\text{sh}}}{0.10z_{\text{sh,ref}}} & \text{if } z_{\text{sh}} \geq 0.9z_{\text{sh,ref}} \end{cases} \quad (\text{XXVI})$$

III Simulation Method

Although the model assumes that the feet and crutches are fixed to the ground, the minimum Coefficient of Friction (CoF) for which this holds can be calculated for each simulated scenario. If in reality the ground CoF is lower than the calculated minimum CoF, the feet or crutches will slip, resulting in an unsuccessful and unsafe STS motion. Therefore, using the minimum CoFs, a feasible region of crutch usage can be defined.

The equations of motion (equation XXVII and XXVIII) can be derived from the kinetic diagram (figure IV). When these equations of motion are solved, the minimum required CoF for the feet ($\mu_{\text{feet,min}}$ in equation XXIX) can be calculated for each time step of the simulation, because the other variables are known. The minimum required CoF for the crutches ($\mu_{\text{crutch,min}}$) can be calculated using the crutch angle for each time step (q_{crutch} in equation XXX defined in figure IV). When the maximum value of all these calculated CoFs is taken, the minimum required CoF to guarantee no slip during the STS motion is known. Comparing the required CoF with the static CoF of rubber with dry concrete between 0.6 and 0.85[20], a feasible STS is stated when the required CoF is below 0.6.

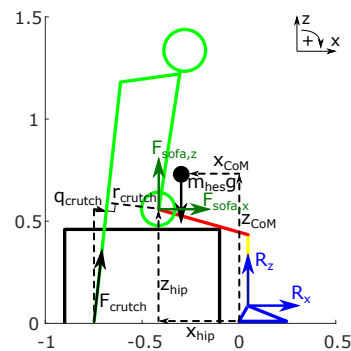


Figure IV: Kinetic diagram of all the forces which are used in the simulation. The black dot represents the CoM of the HES.

$$\sin(q_{\text{crutch}}) F_{\text{crutch}} + F_{\text{sofa},z} + R_z - m_{\text{hes}}g = 0 \quad (\text{XXVII})$$

$$\begin{aligned} R_z(x_{\text{CoM}} - x_{\text{ankle}}) - R_x(z_{\text{CoM}} - z_{\text{ankle}}) \\ + F_{\text{sofa},z}(x_{\text{hip}} - x_{\text{CoM}}) + F_{\text{sofa},x}(z_{\text{hip}} - z_{\text{CoM}}) \\ - F_{\text{crutch}}r_{\text{crutch}} = 0 \quad (\text{XXVIII}) \end{aligned}$$

$$\mu_{\text{feet},\min} = R_x/R_z \quad (\text{XXIX})$$

$$\mu_{\text{crutch},\min} = \arctan(\max(|q_{\text{crutch}}|)) \quad (\text{XXX})$$

The crutch angle, can be defined by the crutch angle with respect to the ground (q_1 in figure V), or with respect to the shoulder (q_2 in figure V). While q_1 is constant over time, q_2 is relative to the shoulder and results in a dynamic angle with respect to the ground.

Using the controller, the HES model, the crutch forces and the sofa interaction, the system can be evaluated for different scenarios. These scenarios are distinguished by the crutch usage in terms of crutch placement, crutch angle (defined by either q_1 or q_2) and crutch force (F_{max} in equation XXIV). The simulations are done with a maximum total crutch force of 600N, which is similar to the maximum crutch force in subject studies[18]. The used stiffness and damping gains are in correspondence to the desired x, z and angle accelerations of 4 m/s^2 , 2 m/s^2 and 4 m/rad^2 (table III). From these simulations the effect of the crutch usage with respect to the slip stability and time performance are identified. When a successful STS motion is defined as reaching the shoulder height of 99% of the reference shoulder height, the success of STS motions can be presented as a result of the crutch usage. When a single scenario is chosen, this scenario can be simulated for different stiffness damper gains (III) to illustrate the effect of these values. All simulations are performed using Matlab's Simulink ODE45 solver with a relative tolerance of $1\text{e-}3$.

IV Results

Simulated scenarios are used to show the effect of the crutches. By computing the minimal required CoF for different crutch placements and crutch angles, a feasible crutch usage region can be determined defined by the determined maximum CoF of 0.6 (figure VI). This feasible crutch usage region will be used to establish an advisable crutch usage region. A constant crutch angle with respect to the ground (q_1 , figure VIa) has a larger feasible region compared to a constant crutch angle with respect to the shoulder angle (q_2 , figure VIb). Furthermore, q_2 shows a larger area where the STS is unsuccessful compared to q_1 . However, both angle definitions show feasible crutch placements below 0.2m behind the heel.

The time performance of the STS motion is also compared using the time until 99% of the reference shoulder height is reached. It can be observed that the time to complete this part of the STS motion is not highly impacted by the crutch usage within the feasible regions and is mostly between 1.5s and 2.5s (figure VII). This is shown

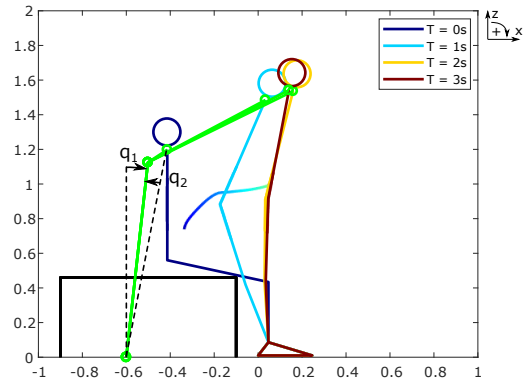


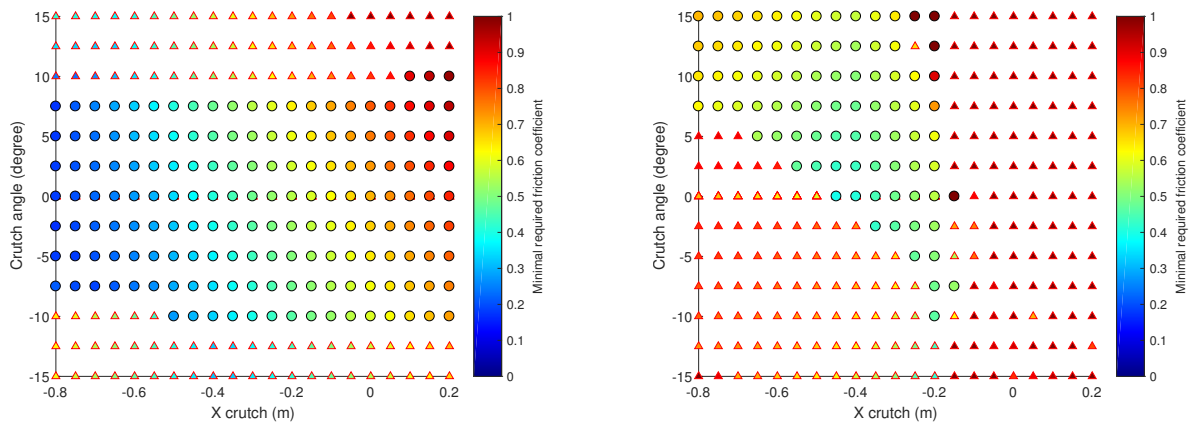
Figure V: Sit to Stand simulation with the CoM trajectory at a constant crutch angle with respect to the ground (q_1) of 5° , the crutch angle with respect to the shoulder (example given for $T = 0\text{s}$) is defined as q_2

by the time performance, which does not vary much when different successful crutch usage scenarios are simulated.

To get more insight in the behaviour of the controller and the modeled crutches, a single scenario is chosen and evaluated. In this single scenario the crutch usage is chosen at a crutch placement of 0.6m behind the heel and a crutch angle defined by q_1 of 5° . This is chosen because both angle definitions shows a successful STS motion at this scenario. The STS motion is evaluated over time. Figure IX shows the time series of the crutch force (figure IXa), desired total joint torques (figure IXb) and joint angles (figure IXc). The used stiffness damper gain values are in correspondence to the desired x, z and angle accelerations of 4 m/s^2 , 2 m/s^2 and 4 m/rad^2 (table III in section II). Figure V shows the simulation of the STS motion for the mentioned scenario.

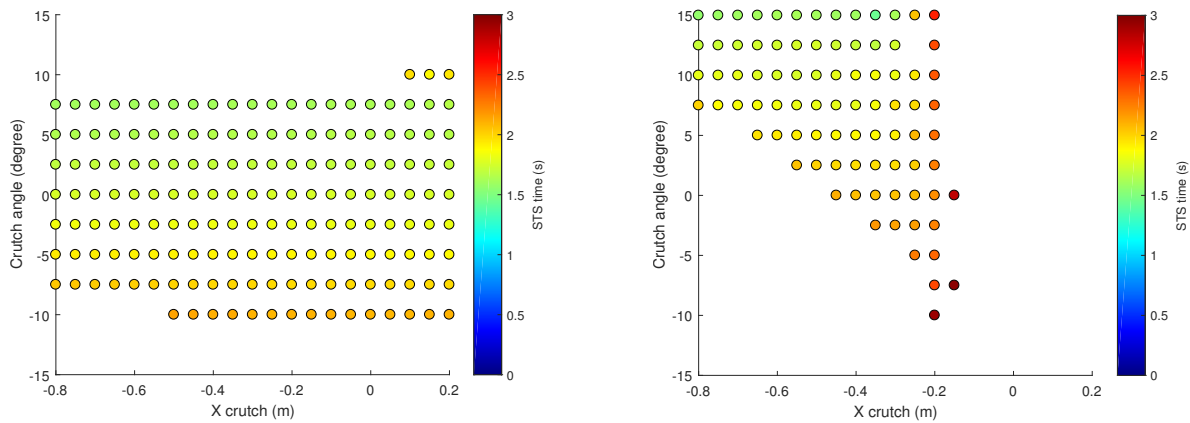
The knee joint reaches its software angle limitation around 0.83s (table II in section II). Therefore, the desired joint torque of the knee (figure IXb) is not directly used as motor input. The knee angle suddenly decelerates, because of this software limitation. As a consequence of the knee angle deceleration, the CoM velocity also changes at that moment in time. This results in a quick (but not instant) change in end-effector (damping) forces and changes the desired joint torques.

Different stiffness-damper gain values are derived from desired accelerations of the end-effector x, z and angle coordinates (table III in section II). The effects of the gain values on the controller can be analyzed for the same crutch usage scenario as evaluated over time ($X_{\text{crutch}} = -0.6\text{m}$ and $q_1 = 5^\circ$). The time needed to reach seat-off and the time needed to reach 99% of the reference shoulder height can be used in combination with the total maximum crutch force to illustrate the effect of the gain values on the STS performance (figure VIII). The total crutch force can be reduced to under 500N for a successful STS motion. when certain gain values are chosen for the specific scenario (figure VIII). Although the time to reach seat-off can be reduced by the gain values (figure VIIIa), the gain values also influence the successfulness of the STS motion (figure VIIIb).



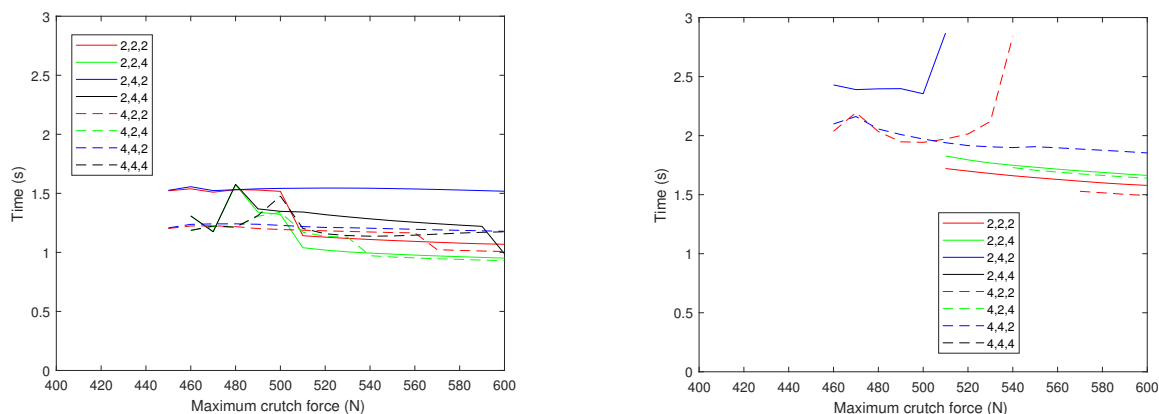
(a) Constant crutch angle with respect to the ground (q_1) (b) Constant crutch angle with respect to the shoulder (q_2)

Figure VI: Minimum required COFs for STS motion simulations of different crutch usage scenario's with a maximum crutch force of 600N. Successful STS motions (defined by reaching 99% of the reference shoulder height) presented as dots and STS motions only reaching the seat-off requirement presented as red lined triangles. The corresponding minimal required CoFs can be seen in the color bar on the side. The used stiffness damper gain values are in correspondence to the desired x , z and angle accelerations of 4 m/s^2 , 2 m/s^2 and 4 m/rad^2 .



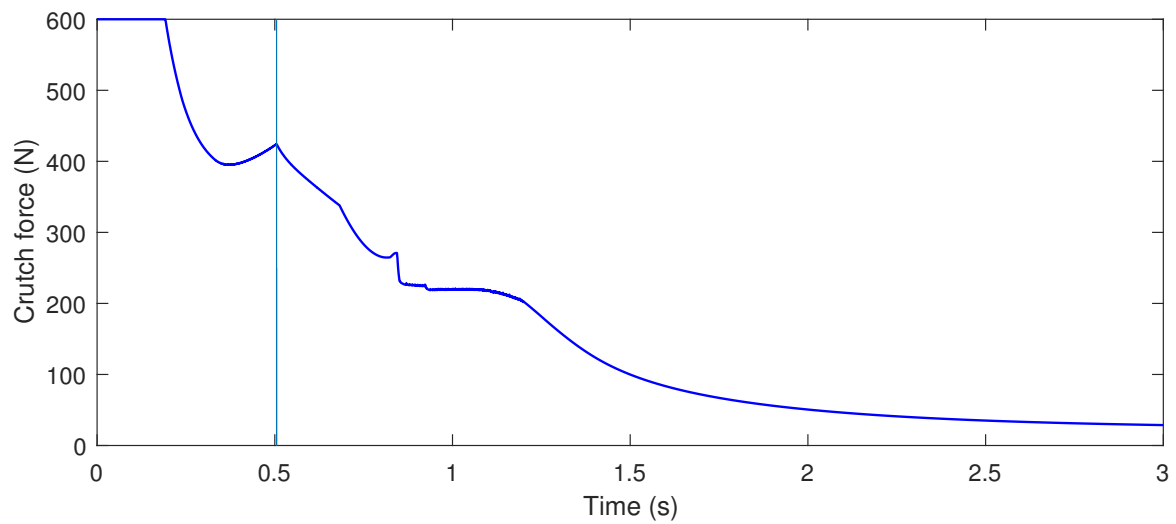
(a) Constant crutch angle with respect to the ground (q_1) (b) Constant crutch angle with respect to the shoulder (q_2)

Figure VII: Time till successful STS for STS simulations of different crutch usage scenario's with a maximum crutch force of 600N. The times corresponding to reaching 99% of the reference shoulder height can be seen in the color bar on the side. The used stiffness damper gain values are in correspondence to the desired x , z and angle accelerations of 4 m/s^2 , 2 m/s^2 and 4 m/rad^2 .

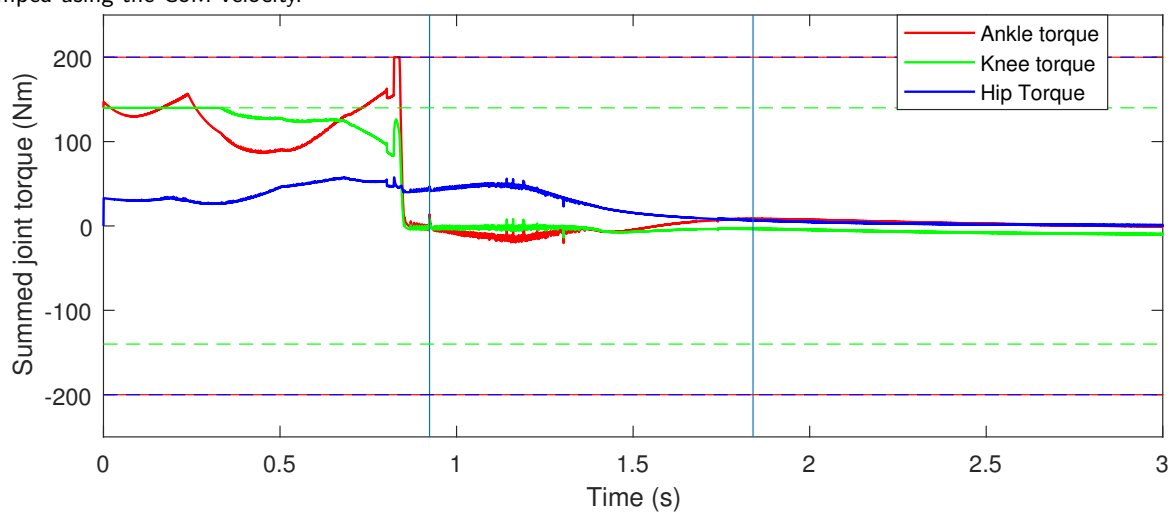


(a) Time till seat-off with respect to maximum crutch force (b) Time till successful STS (reaching 99% of the reference shoulder height) with respect to maximum crutch force

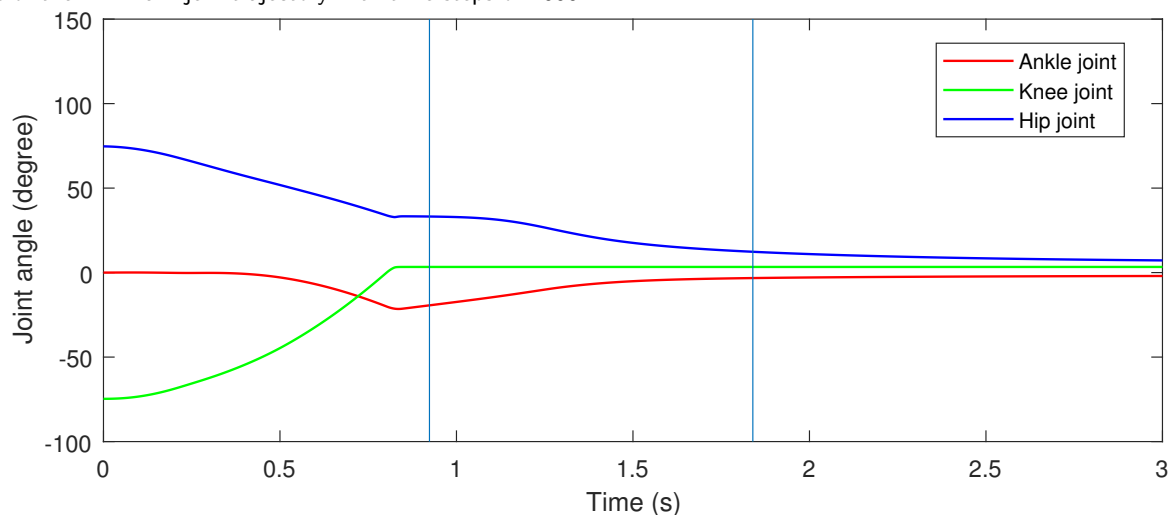
Figure VIII: STS motion performance times with respect to the maximum crutch force for different stiffness and damper gain values using a crutch angle of 5° (q_1) and a crutch placement of 0.6m behind the heel. These gain values are calculated from the desired x , z and angle accelerations of the end-effector. The gains in correspondence with the accelerations of the horizontal, vertical and angle end-effector point of 4m/s^2 , 4m/s^2 and 2m/rad^2 can reduce the performance time and needed crutch force the most.



(a) Time series of total crutch force which decreases after 90% of the reference shoulder height is reached (vertical line) and is damped using the CoM velocity.



(b) Time series of joint torques with the maximum joint torques given by the striped line in the corresponding color. The sudden change in torques around $T = 0.8s$ is a result of the knee joint reaching the software endstop. The small peaks are a result of the minimum jerk trajectory with time steps of 1000Hz.



(c) Time series of joint angles with the knee angle reaching the software endstop around $T = 0.8s$.

Figure IX: Time series for a crutch angle of 5° with respect to the ground placed 0.6m behind the heel with the vertical lines in b) and c) representing the seat-off at 0.92s and reaching 99% of the reference shoulder height at 1.84s

V Discussion

This study presents a successful design of a STS controller for a lower limb exoskeleton, validated using feasible crutch usage identification. This study is the first study presenting a method to determine a feasible operating space of the crutches during STS using computational analysis. This study uses a pace and progress dependent crutch model to validate the controller's design and determine a feasible crutch usage region.

Existing exoskeletons demonstrated successful STS capabilities using crutches[6, 7, 8]. However, the subjects have to be trained in order to use these exoskeletons and crutches correctly. Currently, subjects have different crutch usage strategies learned by trial and error[18]. Although crutch usage preferences of subjects are analyzed, advisable crutch usage strategies are not yet studied[18]. The used method to validate the controller can contribute to an improved training of the STS motion for paraplegic patients using exoskeletons and help therapists by giving advisable crutch usage strategies. Furthermore, the effect of the crutch usage is made more quantifiable and more predictable.

The presented controller uses the angle and angle velocity of the joints. While the angles are measured, the velocity will have to be derived real-time during the usage of the exoskeleton. Although the accelerations can be well approximated in the simulated model, it is chosen not to use the angle accelerations, because in practice the exoskeleton may give inaccurate approximations.

In this study the requirements for stability are expressed as reducing the required CoF until an acceptable value. However, in reality the roll-over of the feet may occur and should also be taken into account. The roll-over of the feet can be analyzed using the zero moment point. However, testing the controller in practice and comparing the advisable crutch usage strategies can give better insights in terms of model validation.

The model used to simulate the crutches is dependent of pace and progress. Here the crutch forces are scaled down if certain threshold are reached. However, subject studies showed that the crutch force does not only scale down, but also takes time to build up[18]. Furthermore, subject studies show that crutch forces show a positive sinusoidal wave pattern and peak during certain moments in time[18]. Although the crutches modeled in this study are dependent on pace and progress, it might still be a too simplistic model to illustrate reality.

To be able to simulate the STS motions, multiple assumptions were made. Although all assumptions are mentioned and elaborated, unaccounted effects can give adverse results when the controller will be used in practice. Therefore, the results presented in this study can only be used as a prediction of the reality.

The controller and model presented in this study can be used to study the effects of different crutch usage strategies. Although this study already presented the effects of crutch usage using a simple crutch model, different crutch models can be used to further study the effect of crutch usage. While this study presented the results of the controller using the technical specifications of the

Wearable Exoskeleton 2, the model can also be used for other exoskeletons after slightly changing the simulated hardware and software limitations. The results found in this study may be used as a rule of thumb for other exoskeletons.

The strength of the controller presented in this study is the ability to perform successful STS motions in a wide variety of crutch usage strategies considering a realistic CoF. Moreover, the used validation method can help to identify proper crutch usage. While it can be useful to know which crutch usage scenarios can positively influence the STS motion, the ability to predict unsuccessful and therefore possible unsafe crutch usage scenarios may be the biggest strength. This study carefully simulated different crutch usage scenarios to identify these positive and negative scenarios.

Future research should focus on improving the model of the crutches and implementing the controller in exoskeletons. By improving the crutch usage model, the influence of the crutches can be further studied, giving more realistic and better crutch usage strategies. These crutch usage strategies can be used to help the training of paraplegic patients using exoskeletons. By implementing the controller into exoskeletons, the controller can be further validated and used to support STS motions.

References

- [1] *International Standards for Neurological Classification of Spinal Cord Injury*, American Spinal Injury Association, 2016. [Online]. Available: http://asia-spinalinjury.org/wp-content/uploads/2016/02/International_Stds_Diagram_Worksheet.pdf
- [2] University of Alabama at Birmingham, *Spinal Cord Injury Facts and Figures at a Glance*, 2018. [Online]. Available: <https://www.nscisc.uab.edu/>
- [3] J. H. B. Nijendijk, M. W. M. Post, and F. W. A. van Asbeck, "Epidemiology of traumatic spinal cord injuries in the netherlands in 2010." *International Spinal Cord Society*, vol. 52, no. 4, pp. 258–263, 2014. [Online]. Available: <https://doi.org/10.1038/sc.2013.180>
- [4] R. Osterthun, M. W. M. Post, and F. van Asbeck, "Characteristics, length of stay and functional outcome of patients with spinal cord injury in dutch and flemish rehabilitation centres." *International spinal Cord Society*, vol. 47, no. 4, pp. 339–344, 2009. [Online]. Available: <https://doi.org/10.1038/sc.2008.127>
- [5] C. Meijneke, S. Wang, V. Sluiter, and H. van der Kooij, "Introducing a modular, personalized exoskeleton for ankle and knee support of individuals with a spinal cord injury," pp. 169–173, 10 2016. [Online]. Available: https://doi.org/10.1007/978-3-319-46532-6_28
- [6] A. Esquenazi, M. Talaty, A. Packel, and M. Saulino, "The rewalk powered exoskeleton to restore ambulatory function to individuals with thoracic-level motor-complete spinal cord injury," *American Journal of Physical Medicine & Rehabilitation*, vol. 91, no. 11, pp. 911 – 921, 2012. [Online]. Available: <https://doi.org/10.1097/PHM.0b013e318269d9a3>
- [7] EksoGT, Ekso Bionics, 2018. [Online]. Available: <http://www.eksobionics.com>
- [8] *Indego exoskeleton*, Parker Hannifin Corp, 2018. [Online]. Available: <http://www.indego.com>
- [9] R. Griffin, T. Cobb, T. Craig, M. Daniel, N. van Dijk, J. Gines, K. Kramer, S. Shah, O. Siebinga, J. Smith, and P. Neuhaus, "Stepping forward with exoskeletons: Team ihmcs design and approach in the 2016 cybathlon," *IEEE Robotics Automation Magazine*, vol. 24, no. 4, pp. 66–74, Dec 2017. [Online]. Available: <https://doi.org/10.1109/MRA.2017.2754284>
- [10] M. Hughes and M. Schenkman, "Chair rise strategy in the functionally impaired elderly," *Journal of rehabilitation research and development*, vol. 33, no. 4, pp. 409–412, 11 1996.
- [11] M. K. Mak, O. Levin, J. Mizrahi, and C. W. Hui-Chan, "Joint torques during sit-to-stand in healthy subjects and people with parkinson's disease," *Clinical Biomechanics*, vol. 18, no. 3, pp. 197 – 206, 2003. [Online]. Available: [https://doi.org/10.1016/S0268-0033\(02\)00191-2](https://doi.org/10.1016/S0268-0033(02)00191-2)
- [12] F. Sibella, M. Galli, M. Romei, A. Montesano, and M. Crivellini, "Biomechanical analysis of sit-to-stand movement in normal and obese subjects," *Clinical Biomechanics*, vol. 18, no. 8, pp. 745 – 750, 2003. [Online]. Available: [https://doi.org/10.1016/S0268-0033\(03\)00144-X](https://doi.org/10.1016/S0268-0033(03)00144-X)
- [13] S. Yoshioka, A. Nagano, R. Himeno, and S. Fukushima, "Computation of the kinematics and the minimum peak joint moments of sit-to-stand movements," *BioMedical Engineering OnLine*, vol. 6, no. 1, p. 26, Jul 2007. [Online]. Available: <https://doi.org/10.1186/1475-925X-6-26>
- [14] G. S. Nikolova and Y. E. Toshev, "Estimation of male and female body segment parameters of the bulgarian population using a 16-segmental mathematical model," *Journal of Biomechanics*, vol. 40, no. 16, pp. 3700 – 3707, 2007. [Online]. Available: <https://doi.org/10.1016/j.jbiomech.2007.06.016>
- [15] A. L. Hof, "The 'extrapolated center of mass' concept suggests a simple control of balance in walking," *Human Movement Science*, vol. 27, no. 1, pp. 112 – 125, 2008. [Online]. Available: <https://doi.org/10.1016/j.humov.2007.08.003>
- [16] C. A. Oatls, "The use of a mechanical model to describe the stiffness and damping characteristics of the knee joint in healthy adults," *Physical Therapy*, vol. 73, no. 11, pp. 10 – 19, 1993. [Online]. Available: <https://doi.org/10.1093/ptj/73.11.740>
- [17] V. K. Kothari and M. K. Gangal, "Assessment of frictional properties of some woven fabrics," *Indian Journal of Fibre and Textile Research*, vol. 19, pp. 151–155, 1994.
- [18] K. Daines, E. D. Lemaire, A. Smith, and A. Herbert-Copley, "Sit-to-stand and stand-to-sit cruth use for lower extremity powered exoskeletons," *IEEE International Symposium on Robotics and Intelligent Sensors (IRIS)*, 2017. [Online]. Available: <https://doi.org/10.1109/IRIS.2017.8250148>
- [19] M. Roebroek, C. Doorenbosch, J. Harlaar, R. Jacobs, and G. Lankhorst, "Biomechanics and muscular activity during sit-to-stand transfer," *Clinical Biomechanics*, vol. 9, no. 4, pp. 235 – 244, 1994. [Online]. Available: [https://doi.org/10.1016/0268-0033\(94\)90004-3](https://doi.org/10.1016/0268-0033(94)90004-3)
- [20] Engineering Toolbox, *Friction and Friction Coefficients*, 2004. [Online]. Available: https://www.engineeringtoolbox.com/friction-coefficients-d_778.html

3 Discussion

Besides the previous discussion, some additional points of discussion can be taken into account when this study is used in future research.

The necessity of making a step during the STS motion is not taken into account in this study. Although the necessity can be predicted using the XCoM or detected using the CoM, stepping is not added in the controller. This is done because the step detection part is a simple rule using the XCoM and most exoskeletons already contain a walking controller. Instead of designing an extra controller to execute the step, the walking controllers can be invoked if this controller is implemented in exoskeletons.

In the presented controller, the torques were added in a simple prioritized manner. Once one of the joints was saturated, the torques were scaled down. It may be useful to use the joints which are saturated differently by using the Nullspace. However, if only one end-effector force is scaled down, which is mostly the case in the simulations, the simple method presented should suffice. It may be possible to find a more effective way to use the motors as efficiently as possible.

Although a global grid-search is used to identify feasible crutch usage strategies, more advanced methods can be used to further optimize the system on different parameters. However, to find a feasible operating space, as presented in the paper, a grid-search should suffice. This because an optimal location and orientation may be found using other methods, but will not be usable due to the disability of the user to follow the exact advised crutch usage.

To reduce the chance of early seat-off, the estimated sofa forces can be subtracted from the gravity balance component. The current design of the controller already pushes the exoskeleton out of the sofa without the vertical stiffness force, because the sofa exerts a force on the HES.

To optimize the controller on user's effort and comfort, the total work can be taken into account. Moreover, the metabolic costs of the user regarding crutch usage can be measured to define the influence of different crutch usage strategies.

Future research should focus on improving the crutch usage model and on implementing the presented controller or results in practice.

References

- [1] M. Hughes and M. Schenkman, "Chair rise strategy in the functionally impaired elderly," *Journal of rehabilitation research and development*, vol. 33, no. 4, pp. 409–412, 11 1996.
- [2] A. J. Young and D. P. Ferris, "State of the art and future directions for lower limb robotic exoskeletons," *IEEE Transactions on Neural Systems and Rehabilitation Engineering*, vol. 25, no. 2, pp. 171–182, Feb 2017. [Online]. Available: <https://doi.org/10.1109/TNSRE.2016.2521160>
- [3] *International Standards for Neurological Classification of Spinal Cord Injury*, American Spinal Injury Association, 2016. [Online]. Available: http://asia-spinalinjury.org/wp-content/uploads/2016/02/International_Std_Diagram_Worksheet.pdf
- [4] J. H. B. Nijendijk, M. W. M. Post, and F. W. A. van Asbeck, "Epidemiology of traumatic spinal cord injuries in the netherlands in 2010." *International Spinal Cord Society*, vol. 52, no. 4, pp. 258–263, 2014. [Online]. Available: <https://doi.org/10.1038/sc.2013.180>
- [5] R. Osterthun, M. W. M. Post, and F. van Asbeck, "Characteristics, length of stay and functional outcome of patients with spinal cord injury in dutch and flemish rehabilitation centres." *International spinal Cord Society*, vol. 47, no. 4, pp. 339–344, 2009. [Online]. Available: <https://doi.org/10.1038/sc.2008.127>
- [6] University of Alabama at Birmingham, *Spinal Cord Injury Facts and Figures at a Glance*, 2018. [Online]. Available: <https://www.nscisc.uab.edu/>
- [7] C. Meijneke, S. Wang, V. Sluiter, and H. van der Kooij, "Introducing a modular, personalized exoskeleton for ankle and knee support of individuals with a spinal cord injury," pp. 169–173, 10 2016. [Online]. Available: https://doi.org/10.1007/978-3-319-46532-6_28
- [8] A. Esquenazi, M. Talaty, A. Packel, and M. Saulino, "The rewalk powered exoskeleton to restore ambulatory function to individuals with thoracic-level motor-complete spinal cord injury," *American Journal of Physical Medicine & Rehabilitation*, vol. 91, no. 11, pp. 911 – 921, 2012. [Online]. Available: <https://doi.org/10.1097/PHM.0b013e318269d9a3>
- [9] EksoGT, Ekso Bionics, 2018. [Online]. Available: <http://www.eksobionics.com>
- [10] *Indego exoskeleton*, Parker Hannifin Corp, 2018. [Online]. Available: <http://www.indego.com>
- [11] R. Griffin, T. Cobb, T. Craig, M. Daniel, N. van Dijk, J. Gines, K. Kramer, S. Shah, O. Siebinga, J. Smith, and P. Neuhaus, "Stepping forward with exoskeletons: Team ihmc's design and approach in the 2016 cybathlon," *IEEE Robotics Automation Magazine*, vol. 24, no. 4, pp. 66–74, Dec 2017. [Online]. Available: <https://doi.org/10.1109/MRA.2017.2754284>
- [12] M. Roebroek, C. Doorenbosch, J. Harlaar, R. Jacobs, and G. Lankhorst, "Biomechanics and muscular activity during sit-to-stand transfer," *Clinical Biomechanics*, vol. 9, no. 4, pp. 235 – 244, 1994. [Online]. Available: [https://doi.org/10.1016/0268-0033\(94\)90004-3](https://doi.org/10.1016/0268-0033(94)90004-3)
- [13] M. K. Mak, O. Levin, J. Mizrahi, and C. W. Hui-Chan, "Joint torques during sit-to-stand in healthy subjects and people with parkinson's disease," *Clinical Biomechanics*, vol. 18, no. 3, pp. 197 – 206, 2003. [Online]. Available: [https://doi.org/10.1016/S0268-0033\(02\)00191-2](https://doi.org/10.1016/S0268-0033(02)00191-2)
- [14] F. Sibella, M. Galli, M. Romei, A. Montesano, and M. Crivellini, "Biomechanical analysis of sit-to-stand movement in normal and obese subjects," *Clinical Biomechanics*, vol. 18, no. 8, pp. 745 – 750, 2003. [Online]. Available: [https://doi.org/10.1016/S0268-0033\(03\)00144-X](https://doi.org/10.1016/S0268-0033(03)00144-X)
- [15] S. Yoshioka, A. Nagano, R. Himeno, and S. Fukashiro, "Computation of the kinematics and the minimum peak joint moments of sit-to-stand movements," *BioMedical Engineering OnLine*, vol. 6, no. 1, p. 26, Jul 2007. [Online]. Available: <https://doi.org/10.1186/1475-925X-6-26>
- [16] T. Yan, M. Cempini, C. M. Oddo, and N. Vitiello, "Review of assistive strategies in powered lower-limb orthoses and exoskeletons," *Robotics and Autonomous Systems*, vol. 64, pp. 120 – 136, 2015. [Online]. Available: <https://doi.org/10.1016/j.robot.2014.09.032>
- [17] M. R. Tucker, J. Olivier, A. Pagel, H. Bleuler, M. Bouri, O. Lambercy, J. d. R. Millán, R. Riener, H. Vallery, and R. Gassert, "Control strategies for active lower extremity prosthetics and orthotics: a review," *Journal of NeuroEngineering and Rehabilitation*, vol. 12, no. 1, p. 1, Jan 2015. [Online]. Available: <https://doi.org/10.1186/1743-0003-12-1>

- [18] C. Dias, M. Sarvi, and M. Iryo-Asano, "Predicting optimal trajectories for constrained pedestrian turning manoeuvres," in *Proc. of the 8th International Conference on Pedestrian and Evacuation Dynamics (PED2016)*, 10 2016.
- [19] L. Wang, E. H. F. van Asseldonk, and H. van der Kooij, "Model predictive control-based gait pattern generation for wearable exoskeletons," in *2011 IEEE International Conference on Rehabilitation Robotics*, June 2011, pp. 1–6. [Online]. Available: <https://doi.org/10.1109/ICORR.2011.5975442>
- [20] B. Chen, C.-H. Zhong, X. Zhao, H. Ma, X. Guan, X. Li, F.-Y. Liang, J. C. Y. Cheng, L. Qin, S.-W. Law, and W.-H. Liao, "A wearable exoskeleton suit for motion assistance to paralysed patients," *Journal of Orthopaedic Translation*, vol. 11, pp. 7 – 18, 2017. [Online]. Available: <https://doi.org/10.1016/j.jot.2017.02.007>
- [21] H. Geyer and H. Herr, "A muscle-reflex model that encodes principles of legged mechanics produces human walking dynamics and muscle activities," *IEEE Transactions on Neural Systems and Rehabilitation Engineering*, vol. 18, no. 3, pp. 263–273, June 2010. [Online]. Available: <https://doi.org/10.1109/TNSRE.2010.2047592>
- [22] A. Wu, F. Dzeladini, T. Brug, F. Tamburella, N. Tagliamonte, E. Van Asseldonk, H. Van Der Kooij, and A. IJspeert, "An adaptive neuromuscular controller for assistive lower-limb exoskeletons: A preliminary study on subjects with spinal cord injury," *Frontiers in neurorobotics*, vol. 11, no. JUN, 6 2017. [Online]. Available: <https://doi.org/10.3389/fnbot.2017.00030>
- [23] O. Narvaez-Aroche, A. Packard, and M. Arcaç, "Motion planning of the sit to stand movement for powered lower limb orthoses," EECS Department, University of California, Berkeley, Tech. Rep. UCB/EECS-2017-148, Oct 2017. [Online]. Available: <https://doi.org/10.1115/DSCC2017-5289>
- [24] V. Rajasekaran, M. Vinagre, and J. Aranda, "Event-based control for sit-to-stand transition using a wearable exoskeleton," in *2017 International Conference on Rehabilitation Robotics (ICORR)*, July 2017, pp. 400–405. [Online]. Available: <https://doi.org/10.1109/ICORR.2017.8009280>
- [25] C. Wu, T. Zhang, Y. Liao, C. Wang, G. Wu, and X. Wu, "Self-adaptive control strategy for exoskeleton to help paraplegic patients stand up and sit down," in *2016 35th Chinese Control Conference (CCC)*, July 2016, pp. 6189–6194. [Online]. Available: <https://doi.org/10.1109/ChiCC.2016.7554328>
- [26] S. Jatsun, S. Savin, and A. Yatsun, "Motion control algorithm for a lower limb exoskeleton based on iterative lqr and zmp method for trajectory generation," in *New Trends in Medical and Service Robots*, M. Husty and M. Hofbauer, Eds. Cham: Springer International Publishing, 2018, pp. 305–317.
- [27] S. Jatsun and S. Savin, "Comparative analysis of iterative lqr and adaptive pd controllers for a lower limb exoskeleton," *IEEE International Conference on Cyber Technology in Automation, Control, and Intelligent Systems*, pp. 239–244, June 2016. [Online]. Available: <https://doi.org/10.1109/CYBER.2016.7574829>
- [28] S. Jatsun, S. Savin, B. Lushnikov, and A. Yatsun, "Algorithm for motion control of an exoskeleton during verticalization," *ITM Web of Conferences*, vol. 6, p. 01001, 2016. [Online]. Available: <https://doi.org/10.1051/itmconf/20160601001>
- [29] A. Herzog, L. Righetti, F. Grimminger, P. Pastor, and S. Schaal, "Momentum-based balance control for torque-controlled humanoids," May 2013. [Online]. Available: <https://doi.org/10.1109/IROS.2014.694267>
- [30] S.-H. Lee and A. Goswami, "A momentum-based balance controller for humanoid robots on non-level and non-stationary ground," *Autonomous Robots*, vol. 33, no. 4, pp. 399–414, 2012. [Online]. Available: <https://doi.org/10.1007/s10514-012-9294-z>
- [31] S. Jatsun, S. Savin, and A. Yatsun, "Parameter optimization for exoskeleton control system using sobol sequences," in *ROMANSY 21 - Robot Design, Dynamics and Control*, V. Parenti-Castelli and W. Schiehlen, Eds. Cham: Springer International Publishing, 2016, pp. 361–368.
- [32] W. Li and E. Todorov, "Iterative linear quadratic regulator design for nonlinear biological movement systems." in *Proceedings of the 1st International Conference on Informatics in Control, Automation and Robotics, (ICINCO 2004)*, vol. 1, 01 2004, pp. 222–229.
- [33] J. Yang, W. H. Chen, and S. Li, "Non-linear disturbance observer-based robust control for systems with mismatched disturbances/uncertainties," *IET Control Theory Applications*, vol. 5, no. 18, pp. 2053–2062, December 2011. [Online]. Available: <https://doi.org/10.1049/iet-cta.2010.0616>
- [34] X. Wei, Z. Guo, and X. Liu, "Composite hierarchical anti-disturbance control for nonlinear robotic systems with robust nonlinear disturbance observer," in *Proceedings of the 32nd Chinese Control Conference*, July 2013, pp. 2694–2699.